FUSION OF ULTRASOUND HARMONIC IMAGING WITH CLUTTER REMOVAL USING SPARSE SIGNAL SEPARATION

Javier S. Turek *Jeremias Sulam* *Michael Elad* *Irad Yavneh*

Department of Computer Science, Technion, Israel Institute of Technology,
Haifa 32000, Israel
{javiert,jsulam,elad,irad}@cs.technion.ac.il

ABSTRACT

In ultrasound, second harmonic imaging is usually preferred due to the higher clutter artifacts and speckle noise common in the first harmonic image. Typical ultrasound use either one or the other image, applying corresponding filters for each case. In this work we propose a method based on a joint sparsity model that fuses the first and second harmonic images while performing clutter mitigation and noise reduction. Our approach, Fused Morphological Component Analysis (FMCA), uses two adaptive dictionaries for characterizing the clutter components in each image, and a common dictionary for the tissue representation. Our results indicate that the obtained images contain less clutter artifacts, less speckle noise and as such enjoy of the benefits of both harmonic input images.

Index Terms— Artifact reduction, signal separation, harmonic imaging, image fusion, morphological component analysis

1. INTRODUCTION

Ultrasound imaging is one of the most important medical imaging modalities, performed by acquiring the reflected ultrasound waves from the inner tissues. Although this modality is able to provide portable, online imaging with no radiation, it also suffers from several limitations, such as low resolution, low signal to noise ratio due to the multiplicative speckle noise, and other artifacts. In echocardiography in particular, the use of tissue harmonic imaging has been shown to improve the image quality [1]. Acquiring the second or higher harmonics instead of the reflected signals in the fundamental frequency enables suppressed side and grating lobes and minimal harmonic content in reverberant echoes. These contribute to a cleaner image with less artifacts and higher resolution. However, this comes at the cost of lower penetration depth and intensity [1, 2].

The research leading to these results has received funding from the European Research Council under European Union's Seventh Framework Programme, ERC Grant agreement no. 320649.

This work was partially supported by MAGNETON project from the Office of the Chief Scientist [OCS] in the Israeli Ministry of Economy.

An important class of artifact in ultrasound imaging is that of clutter, which appears mainly as a quasi-static cloud of echo signals [3]. This problem is most severe in patients for whom the acquisition conditions are difficult [4]. Such artifacts obscure tissue areas and the resulting image has poor contrast and reduced readability. Therefore, it can mislead to corrupt diagnostic information like in myocardium strain evaluation [5], tracking techniques for functioning diagnosis [6], or visualization of cardiac abnormalities [7]. Cluttering is most prominent in fundamental frequency imaging, requiring aggressive filtering techniques, while it is usually reduced using harmonic imaging. Nevertheless, in some cases clutter is still present in the second harmonic image [8], requiring additional processing.

Some typical schemes for clutter mitigation involve linear filtering and transformation onto unitary bases such as the Discrete Fourier Transform [9] and Wavelets [10]. More effective methods are based on adaptive bases learned from the echo data, such as Principal Component Analysis (PCA) [11]. A different approach is that of Morphological Component Analysis (MCA), as suggested in [12] and [13], where the separation of the signals is done by means of an adaptive redundant non-orthonormal basis or *dictionary*.

Image fusion in medical imaging is an approach that seeks to combine the benefits of different medical imaging modalities to enhance salient features [14]. In ultrasound imaging in particular, one can consider fusion of several harmonic imaging bands. Indeed, the work reported in [15] considers such fusion directed towards superresolution.

In the last decade, sparsity related ideas have had a growing impact on image processing applications [16]. In this work we propose a method of fusing the first and second harmonic images while performing clutter mitigation based on joint sparse representations. We propose a model that enforces joint sparsity on the tissue component of both fundamental and second harmonic images, while allowing the removal of clutter from both of them simultaneously. As described later, this yields a cleaner image in terms of clutter and speckle noise removal, while providing a fused image which enjoys the benefits of both ultrasound harmonics.

2. SPARSE REPRESENTATIONS OF SIGNALS

A signal $\mathbf{t} \in \mathbb{C}^{\mathrm{n}}$ is said to have a sparse representation over a known overcomplete dictionary $\mathbf{D} \in \mathbb{C}^{\mathrm{n}\times\mathrm{m}}$ if there exists a sparse vector $\mathbf{x} \in \mathbb{C}^{\mathrm{m}}$, such that $\mathbf{t} = \mathbf{D}\mathbf{x}$ and $\|\mathbf{x}\|_0 = k \ll n$. Here, $\|\cdot\|_0$ denotes the ℓ_0 quasi-norm, which is the number of non-zero elements in a vector. In practice, an observed signal $\mathbf{s}$ is obtained by measuring a signal of interest $\mathbf{t}$ contaminated with noise $\mathbf{v}$, which is often assumed to be additive WGN with standard deviation σ, i.e., $\mathbf{s} = \mathbf{t} + \mathbf{v}$. The objective is to recover the signal $\mathbf{t}$ from the noisy observation $\mathbf{s}$. Assuming a sparse representation prior on the signal $\mathbf{t}$, one can redefine the observed signal as $\mathbf{s} = \mathbf{D}\mathbf{x} + \mathbf{v}$. Then, $\mathbf{x}$ is computed by solving the following optimization problem:

$$\min_{\mathbf{x}} \|\mathbf{s} - \mathbf{D}\mathbf{x}\|_2^2 \quad s.t. \quad \|\mathbf{x}\|_0 \leq k. \tag{1}$$

where k is the maximum number of non-zeros allowed in the representation. Once the sparse vector $\hat{\mathbf{x}}$ has been obtained, the estimate of the clean is computed by multiplying the dictionary $\mathbf{D}$ by $\hat{\mathbf{x}}$. Several methods exist to compute an approximate solution $\hat{\mathbf{x}}$ to Problem (1), one being the greedy pursuit algorithm called Orthogonal Matching Pursuit (OMP) [17]. An alternative is to relax the ℓ_0-norm with the ℓ_1-norm, obtaining the convex Basis Pursuit problem [18] which can be solved using standard optimization algorithms. The OMP has proven to be an affective compromise between accuracy and computational cost [19] and it will be used in our work when solving Problem (1).

The choice of the dictionary $\mathbf{D}$ is of great importance in obtaining the sparse vector $\mathbf{x}$. Though computationally efficient, dictionaries that are mathematically pre-defined are limited in terms of approximation performance [19]. Alternatively, the dictionary can be learned adaptively from the data to yield better results. Amongst these, the K-SVD [20] algorithm is a commonly used method for dictionary learning, which has proven to be effective in several image processing applications [16].

3. HARMONIC IMAGING FUSION WITH SPARSE SIGNAL SEPARATION

The echo waves correspond to a linear phenomena. Hence, and following our previous work in [12, 13], we assume that the acquired signal is the linear combination of echoes reflected by tissue, reverberation artifacts (clutter) and measurement noise:

$$\mathbf{s} = \mathbf{t} + \mathbf{c} + \mathbf{v}, \tag{2}$$

where $\mathbf{t}$ is the tissue signal and $\mathbf{c}$ represents the clutter artifacts. In order to construct the training signals we divide the data into small overlapping patches and apply the separation and fusion scheme to these small patches. We take each sample signal $\mathbf{s}^i$ as a two-dimensional patch in the axial and temporal dimensions[1] from the observed signal $\mathbf{s}$, enabling the study of the temporal characteristics (static/moving) of a patch. That is, a signal $\mathbf{s}^i$ is a vectorized version of a two dimensional patch of M elements across the axial direction and N elements (frames) in the temporal direction. The size N influences the amount of motion that is captured by the patches[2]. The assumptions above about the signal model remain true also for each patch, and hence Eq. (4) is applicable to the patches $\mathbf{s}^i$:

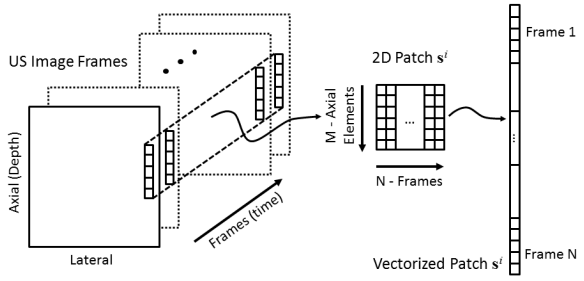

Fig. 1: Diagram describing the process of data construction from the sequence of echo images. Each signal $\mathbf{s}^i$ is a columnized version of a two dimensional patch in the axial and temporal directions.

$$\mathbf{s}^i = \mathbf{t}^i + \mathbf{c}^i + \mathbf{v}^i. \tag{3}$$

Assuming that the tissue and the clutter signals have sparse representations $\mathbf{x}_t^i$ and $\mathbf{x}_c^i$, under dictionaries $\mathbf{D}_t$ and $\mathbf{D}_c$, respectively, we may rewrite (3) as

$$\mathbf{s}^i = \mathbf{D}_t\mathbf{x}_t^i + \mathbf{D}_c\mathbf{x}_c^i + \mathbf{v}^i = [\mathbf{D}_t|\mathbf{D}_c] \cdot \begin{bmatrix} \mathbf{x}_t^i \\ \mathbf{x}_c^i \end{bmatrix} + \mathbf{v}^i = \mathbf{D}\mathbf{x}^i + \mathbf{v}^i, \tag{4}$$

where $\mathbf{D}$ is a dictionary constructed by concatenating both dictionaries $\mathbf{D}_t$ and $\mathbf{D}_c$, and $\mathbf{x}^i$ represents the concatenation of the sparse representations of the tissue and clutter components. When a signal can be decomposed into two or more separate components having a sparse representation under different dictionaries, they can be separated through the scheme in Eq. (4), which is known as Morphological Component Analysis (MCA) [21]. Hence, the clutter component can be filtered by obtaining $\mathbf{x}^i$ and then removing the coefficients corresponding to the clutter as

$$\hat{\mathbf{s}}^i = \mathbf{s}^i - \mathbf{D}_c\mathbf{x}_c^i = \mathbf{D}_t\mathbf{x}_t^i + \mathbf{v}^i, \tag{5}$$

where $\hat{\mathbf{s}}^i$ is the clutter-filtered version of the patch vector $\mathbf{s}^i$. Note that a different alternative would be to reconstruct $\hat{\mathbf{s}}^i$ considering just the tissue component. This way, however, some small and fast moving structures might be confused with noise and would be removed. Thus, we employ Eq. (5).

[1] The echo data can be taken as a three dimensional element, by adding consecutive axial lines to every signal $\mathbf{s}^i$ and thus including information in the lateral direction.

[2] For a given time lapse, the faster the frame rate the bigger the size N needs to be in order to capture the same amount of information.

While this signal model has proven useful in previous works [12, 13], we extend the model in Eq. (4) into a jointly sparse morphological analysis by considering signals $\mathbf{s}_1$ and $\mathbf{s}_2$ corresponding to the first and second harmonic images, respectively, and their corresponding aligned patches $\mathbf{s}_1^i$ and $\mathbf{s}_2^i$. Using the fact that the tissue component in both images has the same source [15], we can enforce these components to have the same sparse representation under the tissue dictionary $\mathbf{D}_t$. On the other hand, the clutter components will differ due to the different phenomena generating these artifacts in each frequency range [1]. This motivates us to propose the following signal model:

$$\begin{bmatrix} \mathbf{s}_1^i \\ \hline \mathbf{s}_2^i \end{bmatrix} = \left[\begin{array}{c|c|c} \mathbf{D}_t & \mathbf{D}_{c1} & \mathbf{0} \\ \hline \mathbf{D}_t & \mathbf{0} & \mathbf{D}_{c2} \end{array}\right] \begin{bmatrix} \mathbf{x}_t^i \\ \hline \mathbf{x}_{c1}^i \\ \hline \mathbf{x}_{c2}^i \end{bmatrix} + \mathbf{v}^i, \qquad (6)$$

where the expression in the left-hand side accounts for the concatenation of the signal vectors, while $\mathbf{D}_{c1}$ and $\mathbf{D}_{c2}$ are the dictionaries of the clutter components of the first and second harmonics, respectively. These clutter dictionaries are concatenated with the tissue dictionary $\mathbf{D}_t$ and two zero matrices to form the complete dictionary. This way, the sparse representation of the tissue components are jointly coded into the top elements of $\mathbf{x}$, namely $\mathbf{x}_t^i$, while the clutter components are allowed to differ, and similarly the noise components. Armed with these elements, we compute an equivalent of Eq. (5) for each of the signals $\mathbf{s}_1^i$ and $\mathbf{s}_2^i$, and obtain the fused patches as [3]:

$$\hat{\mathbf{s}}_f^i = \frac{\hat{\mathbf{s}}_1^i + \hat{\mathbf{s}}_2^i}{2} = \mathbf{D}_t \mathbf{x}_t^i + \frac{1}{2}(\mathbf{v}_1^i + \mathbf{v}_2^i). \qquad (7)$$

The dictionaries involved may be selected a-priori based on the characteristics of the components, or may be trained on real data instead. We follow a similar approach to that of [13], and train the clutter dictionaries $\mathbf{D}_{c1}$ and $\mathbf{D}_{c2}$ on real data taken from the right side of the chest with the K-SVD algorithm, from the first and second harmonics respectively. This alternative takes advantage of the fact that the right side of the chest has a similar physical structure to that of the left side (ribs and lungs), with the exception that there are no echoes returning from the heart. Also, since the atoms are trained on the reverberations from the ribs, this method enables us to train a clutter dictionary off-line, which fits all patients.

For the tissue dictionary $\mathbf{D}_t$, we propose a scheme that naturally incorporates information from both harmonic images by training the dictionary on the average of both signals $(\mathbf{s}_1 + \mathbf{s}_2)/2$. However, since these images contain clutter artifacts, some atoms in the resulting dictionary will correspond to this static behavior. In order to *clean* these atoms, we seek among them those that are well represented by the clutter dictionary $\mathbf{D}_{c2}$[4], essentially applying OMP on each of them with a sparsity constraint of M obtaining corresponding representations γ^j. Then, we remove from $\mathbf{D}_t$ those atoms $\mathbf{d}_t^j$ which satisfy with the following condition:

$$||\mathbf{d}_t^j - \mathbf{D}_{c2}\,\gamma^j||_2 \leq \epsilon, \qquad (8)$$

where ϵ is a threshold parameter set empirically as 0.2.

After the sparse representation $\mathbf{x}^i$ for each patch is computed, the clutter is removed per patch as exposed in Eq. (5). Then, the clean patches are merged together using Eq. (7), and finally the fused patches are averaged to reconstruct the output image. We dub this method Fused Morphological Component Analysis (FMCA).

4. EXPERIMENTS AND RESULTS

In this section we demonstrate our method using two data sets of In-phase Quadrature (IQ) echo data acquired from a parasternal long axis view of two adult male volunteers. The sequences contain a full heart cycle (40-50 frames) and were acquired using a Vivid S6 (GE Medical Systems, Israel) ultrasound scanner transmitting at a frequency of 1.7 MHz. The fundamental and the second harmonic signals are received simultaneously at 1.7 and 3.4 MHz respectively, and separated later with a bandwidth of 0.7 MHz for the first harmonic and 1 MHz for the second harmonic. The images are of reduced quality due to limitations of the simultaneous acquisition of both harmonic signals. Clutter artifacts are present due to multi-path reverberations, mainly from the thoracic cage and sternum. Our implementation uses full-overlapping 15×15 patches, with clutter dictionaries of 248 atoms each, and a tissue dictionary of 900 atoms (before the cleaning stage in Eq. (8) with $\epsilon = 0.2$). We used 10 iterations for K-SVD.

The amount of clutter removed from an echo frame is quantified by the Contrast-to-Noise-Ratio (CNR) [11] measure:

$$\text{CNR} = 20 \log_{10} \left(\frac{|\mu_i - \mu_0|}{\sigma_0} \right), \qquad (9)$$

where μ_i and μ_0 are the mean envelope-detected quantities in regions with and without clutter artifacts (marked with magenta and blue rectangles in Fig. 2a, respectively), and σ_0 is the standard deviation in the clutter-empty region. Then, the mean CNR performance for an entire sequence is obtained by averaging the CNR across frames.

In order to quantify the reduction of speckle noise we measure the Spatial Standard Deviation (SSD) within a homogeneous region chosen in the interior of the ventricle where no tissue is to be expected. The SSD is computed for each frame and then averaged along the time direction.

In Fig. 2 we present the two harmonic images taken from dataset 1 ((a) and (b), where the clutter is marked with a red

[3] Note that the signals $\mathbf{s}_1$ and $\mathbf{s}_2$ have been previously normalized to have the same energy. Otherwise we would need to introduce weighting in (7).

[4] The dictionary $\mathbf{D}_{c1}$ could have been used as well. No significant difference was observed in our experiments.

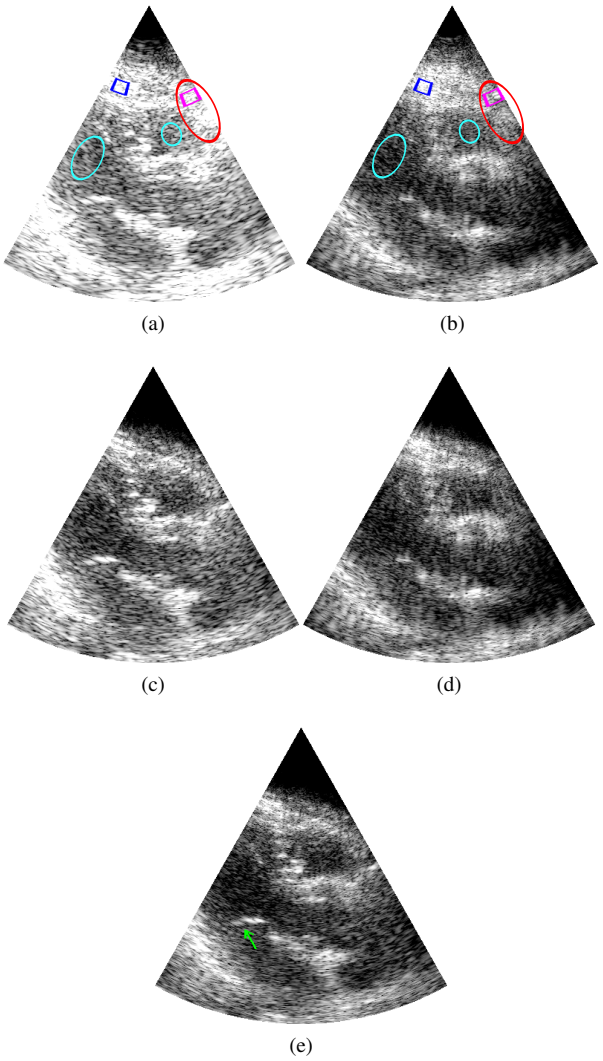

Fig. 2: Examples of images from the first (a) and second (b) harmonics, their corresponding filtered versions $\hat{\mathbf{s}}_1$ and $\hat{\mathbf{s}}_2$ ((c) and (d), respectively), and the FMCA output image $\hat{\mathbf{s}}_f$ (e).

ellipse and ventricle areas with speckle noise with cyan ellipses), the corresponding clean images $\hat{\mathbf{s}}_1$ and $\hat{\mathbf{s}}_2$, and the output image $\hat{\mathbf{s}}_f$ in (e). It can be appreciated that $\hat{\mathbf{s}}_f$ has been filtered effectively from clutter, and also contains considerably less speckle noise. The resolution achieved is somewhat in between that of the first and of the second harmonics. Note how structures such as the mitral valve have been enhanced by the proposed method, as shown by the green arrow. The images from data set 2 exhibit similar results, and thus we reproduce only the first one due to space limitations.

The quantitative results in terms of mean CNR are depicted in Table 1, where we also compare with the method of [13]. In that work, the authors propose a Tissue Adaptive-MCA (TA-MCA) based on an off-line trained dictionary for the clutter component and a tissue adaptive dictionary for the tissue component. We thus apply TA-MCA for cluttering removal to the first and second harmonic images independently,

	Dataset 1	**Dataset 2**
Orig. 1st Harm.	-2.84	-6.11
Orig. 2nd Harm.	0.01	-1.51
TA-MCA 1st Harm.	1.23	-2.28
TA-MCA 2nd Harm.	2.46	0.30
TA-MCA Compounded	1.57	-1.28
TA-MCA Improvement	3.87	2.85
FMCA 1st Harm.	1.87	-1.43
FMCA 2nd Harm.	2.59	0.25
FMCA Compounded	2.24	-0.52
FMCA Improvement	**4.54**	**3.61**

Table 1: Mean CNR results over two datasets [dB].

	Dataset 1		**Dataset 2**	
Region	1	2	1	2
Orig. 1st Harm.	53.37	44.20	24.20	28.67
Orig. 2nd Harm.	23.02	19.84	11.99	16.57
TA-MCA 1st Harm.	42.16	26.46	16.52	18.49
TA-MCA 2nd Harm.	19.86	13.55	8.40	11.82
TA-MCA Compounded	23.18	14.91	9.24	10.95
FMCA 1st Harm.	23.25	15.39	10.42	11.14
FMCA 2nd Harm.	18.05	12.43	7.21	10.50
FMCA Compounded	**15.58**	**10.48**	**6.61**	**8.14**

Table 2: Mean SSD results over two regions in each dataset.

and present the results over the averaged version of these outcomes for the sake of comparison. We also include the relative improvements over the average of the original first and second harmonic images. Our approach of combining the information of the first and second harmonic within the separation task allows the better coding of the sparse representations corresponding to the tissue, therefore enabling better filtering of the clutter, as evidenced by the results.

The speckle noise reduction in terms of the SSD can be appreciated in Table 2. Our method exploits the joint coding of the information in both harmonic images and obtains a speckle noise component which is comparable to the filtered second harmonic. Moreover, note that our results have considerably less speckle noise than TA-MCA compounded (averaged) due to the improvements of the joint sparse coding.

5. CONCLUSIONS

We have presented a method that exploits the information shared by the first and second harmonic imaging by using a jointly sparse model. Our method makes use of dictionaries that allow to perform clutter filtering through morphological component analysis simultaneously in both harmonics and fuses the resulting images to reduce speckle noise while enhancing the tissue details. FMCA achieved better cluttering removal performance together with speckle noise reduction in the studied datasets. A broader validation would contribute to the understanding of the limitations of the method. Finally, a similar scheme may be beneficial in other medical imaging modalities.

6. ACKNOWLEDGMENTS

The authors would like to thank G.E. Medical Systems, Israel for their kind help and technical support.

7. REFERENCES

[1] J. D. Thomas and D. N. Rubin, "Tissue harmonic imaging: Why does it work?," *Journal of the American Society of Echocardiography*, vol. 11, no. 8, pp. 803–808, Aug. 1998.

[2] F. Tranquart, N. Grenier, V. Eder, and L. Pourcelot, "Clinical use of ultrasound tissue harmonic imaging," *Ultrasound in Medicine and Biology*, vol. 25, no. 6, pp. 889 – 894, 1999.

[3] M.A. Lediju, M.J. Pihl, S.J. Hsu, J.J. Dahl, C.M. Gallippi, and G.E. Trahey, "Magnitude, origins, and reduction of abdominal ultrasonic clutter," in *IEEE International Ultrasonics Symposium (IUS)*, Nov. 2008, pp. 50–53.

[4] M.A. Lediju, M.J. Pihl, S.J. Hsu, J.J. Dahl, C.M. Gallippi, and G.E. Trahey, "A motion-based approach to abdominal clutter reduction," *IEEE Trans. Ultrason., Ferroelectr., Freq. Control*, vol. 56, no. 11, pp. 2437–2449, Nov. 2009.

[5] A. Teske, B. De Boeck, P. Melman, G. Sieswerda, P. Doevendans, and M. Cramer, "Echocardiographic quantification of myocardial function using tissue deformation imaging, a guide to image acquisition and analysis using tissue doppler and speckle tracking," *Cardiovascular Ultrasound*, vol. 5, no. 1, pp. 27, 2007.

[6] M. Tanabe, B. Lamia, H. Tanaka, D. Schwartzman, M. R. Pinsky, and J. Gorcsan III, "Echocardiographic speckle tracking radial strain imaging to assess ventricular dyssynchrony in a pacing model of resynchronization therapy," *Journal of the American Society of Echocardiography*, vol. 21, no. 12, pp. 1382–1388, 2008.

[7] D. Mele, O. Soukhomovskaia, E. Pacchioni, E. Merli, N. Avigni, L. Federici, R. A. Levine, and R. Ferrari, "Improved detection of left ventricular thrombi and spontaneous echocontrast by tissue harmonic imaging in patients with myocardial infarction," *Journal of the American Society of Echocardiography*, vol. 19, pp. 1373–1381, Nov. 2006.

[8] C. Caiati, N. Zedda, C. Montaldo, R. Montisci, and S. Iliceto, "Contrast-enhanced transthoracic second harmonic echo doppler with adenosine: A noninvasive, rapid and effective method for coronary flow reserve assessment," *Journal of the American College of Cardiology*, vol. 34, no. 1, pp. 122 – 130, 1999.

[9] S. Bjaerum, H. Torp, and K. Kristoffersen, "Clutter filter design for ultrasound color flow imaging," *IEEE Trans. Ultrason., Ferroelectr., Freq. Control*, vol. 49, no. 2, pp. 204–216, Feb. 2002.

[10] P. C. Tay, S. T. Acton, and J. A. Hossack, "A wavelet thresholding method to reduce ultrasound artifacts," *Computerized Medical Imaging and Graphics*, vol. 35, no. 1, pp. 42–50, 2011.

[11] F.W. Mauldin, D. Lin, and J.A. Hossack, "The singular value filter: A general filter design strategy for PCA-based signal separation in medical ultrasound imaging," *IEEE Trans. Med. Imag.*, vol. 30, no. 11, pp. 1951–1964, Nov. 2011.

[12] J. S. Turek, M. Elad, and I. Yavneh, "Clutter mitigation in echocardiography using sparse signal separation," *Submitted to Int. Journal in Biomedical Imaging*, 2014.

[13] J. S. Turek, M. Elad, and I. Yavneh, "Sparse signal separation with an off-line learned dictionary for clutter reduction in echocardiography," in *To appear in IEEE 28-th Convention of Electrical and Electronics Engineers in Israel 2014*, Dec. 2014.

[14] S. Li, H. Yin, and L. Fang, "Group-sparse representation with dictionary learning for medical image denoising and fusion," *IEEE Trans. Biomed. Eng.*, vol. 59, no. 12, pp. 3450–3459, Dec. 2012.

[15] T. Taxt and R. Jirik, "Superresolution of ultrasound images using the first and second harmonic signal," *IEEE Trans. Ultrason., Ferroelectr., Freq. Control*, vol. 51, no. 2, pp. 163–175, Feb. 2004.

[16] A. Bruckstein, D. Donoho, and M. Elad, "From sparse solutions of systems of equations to sparse modeling of signals and images," *SIAM Review*, vol. 51, no. 1, pp. 34–81, 2009.

[17] S.G. Mallat and Z. Zhang, "Matching pursuits with time-frequency dictionaries," *IEEE Trans. Signal Process.*, vol. 41, no. 12, pp. 3397–3415, Dec. 1993.

[18] S. Chen, D. Donoho, and M. Saunders, "Atomic decomposition by basis pursuit," *SIAM Journal on Scientific Computing*, vol. 20, no. 1, pp. 33–61, 1998.

[19] R. Rubinstein, A. M. Bruckstein, and M. Elad, "Dictionaries for sparse representation modeling," *Proc. IEEE*, vol. 98, no. 6, pp. 1045–1057, Jun. 2010.

[20] M. Aharon, M. Elad, and A. Bruckstein, "K-SVD: An algorithm for designing overcomplete dictionaries for sparse representation," *IEEE Trans. Signal Process.*, vol. 54, no. 11, pp. 4311–4322, Nov. 2006.

[21] J.-L. Starck, M. Elad, and D. Donoho, "Redundant multiscale transforms and their application for morphological component separation," in *Advances in Imaging and Electron Physics*, vol. 132, pp. 287–348. 2004.